Lab on a Chip

Distance-Based Paper Analytical Device for Multiplexed Quantification of Cytokine Biomarkers Using Carbon Dots Integrated with Molecularly Imprinted Polymer

Journal:	*Lab on a Chip*
Manuscript ID	LC-ART-01-2024-000055.R1
Article Type:	Paper
Date Submitted by the Author:	02-Mar-2024
Complete List of Authors:	Khachornsakkul, Kawin; Tufts University, Electrical and Computer Engineering Del-Rio-Ruiz, Ruben; Tufts University, Department of Electrical and Computer Engineering; Tufts University, Nanolab Chheang, Lita; Tufts University, Electrical and Computer Engineering; KMUTT, Chemistry Zeng, Wenxin; Tufts University, Department of Electrical and Computer Engineering; Tufts University, Nanolab Sonkusale, Sameer; Tufts University, Department of Electrical and Computer Engineering; Tufts University, Nanolab

Distance-Based Paper Analytical Device for Multiplexed Quantification of Cytokine Biomarkers Using Carbon Dots Integrated with Molecularly Imprinted Polymer

Kawin Khachornsakkul,[1,2*] Ruben Del-Rio-Ruiz,[1,2] Lita Chheang,[1,2,3] Wenxin Zeng,[1,2] Sameer Sonkusale[1,2*]

[1] *Department of Electrical and Computer Engineering, Tufts University, Medford, MA 02155, USA*

[2] *Nano Lab, Tufts University, Medford, MA 02155, USA*

[3] *Department of Chemistry, Faculty of Science, King Mongkut's University of Technology Thonburi, Bangkok 10140, Thailand*

**To whom correspondence should be addressed. Email: Kawin.khachornsakkul@tufts.edu sameer.sonkusale@tufts.edu*

Abstract

This article introduces distance-based paper analytical devices (dPADs) integrated with molecularly imprinted polymers (MIPs) and carbon dots (CDs) for simultaneous quantification of cytokine biomarkers, namely C-reactive protein (CRP), Tumor Necrosis Factor-alpha (TNF-α), and interleukin-6 (IL-6) in human biologicals samples for diagnosis of cytokine syndrome. Use of fluorescent CDs and MIP technology, the dPAD exhibits high selectivity and sensitivity. Detection is based on fluorescence quenching of CDs achieved through the interaction of the target analytes with the MIP layer on the paper substrate. Quantitative analysis is easily accomplished by measuring the distance length of quenched fluorescence with a traditional ruler and naked eye readout enabling rapid diagnosis of the cytokine syndrome and the underlying infection. Our sensor demonstrated linear ranges of 2.50-24.0 pg mL^{-1} (R^2 = 0.9974), 0.25-3.20 pg mL^{-1} (R^2 = 0.9985), and 1.50-16.0 pg mL^{-1} (R^2 = 0.9966) with detection limits (LODs) of 2.50, 0.25, 1.50 pg mL^{-1} for CRP, TNF-α, and IL-6, respectively. This sensor also demonstrated remarkable selectivity compared to sensor employed using non-imprinted polymer (NIP), and precision with the highest relative standard deviation (RSD) of 5.14%. The sensor is more accessible compared to prior methods relying on expensive reagents and instruments and complex fabrication methods. Furthermore, the assay provided markable accuracy for monitoring these biomarkers in various human samples with recovery percentages ranging between 99.22 and 103.58%. By integrating microfluidic systems, nanosensing, and MIPs technology, our developed dPADs holds significant potential as a cost-effective and user-friendly analytical method for point-of-care diagnostics (POC) of cytokine-related disorders. This concept can be further extended to developing diagnostic device for other biomarkers.

Keywords: Distance-based paper analytical devices (dPADs), carbon dots, molecular imprinted polymers (MIPs), point-of-care diagnostics (POC), fluorescence, cytokine biomarkers

The human immune system is a sophisticated interplay of diverse cellular components collaborating to protect and remedy our body against diseases by combatting antigens and pathogens and controlling infections and their associated symptoms.[1] Cytokines play a crucial role in human immunology by mediating communication between various cells to bolster the immune response.[2,3] Monitoring cytokine levels within the body is of tremendous value for clinical diagnosis and prognosis because they are associated with several diseases, including but not limited to inflammation, infection, injury, myocardial infarction, diabetes, Alzheimer's, Parkinson's disease, sepsis, asthma, heart disease, rheumatoid arthritis, Acquired Immune Deficiency Syndrome (AIDS), depression, and various cancers.[4-7] More recently, elevated serum cytokine levels have emerged as a crucial indicator for assessing the severity of COVID-19 as their production significantly increases upon infection leading to the immune response collapse known as a cytokine storm.[7,8] This phenomenon is not limited to COVID-19 and extends to other infections and cancers, often with life-threatening consequences. Cytokine biomarkers also play a vital role in a wide range of medical conditions, offering clinicians valuable insights for accurate diagnosis and informed treatment decisions. The most common sensor for quantification of cytokines relies on immunological analysis, such as enzyme-linked immunosorbent assay (ELISA) and lateral flow immunoassay (LFIA).[9-11] While such ELISA methods provide great selectivity and sensitivity, they can only be operated by a skilled-user requiring sufficient sample preparation and analysis time. Moreover, the instruments for quantitative monitoring using these methods might not be accessible to resource-limited settings for diagnosis and prognosis. Similarly, although conventional LFIA is a promising diagnostic tool, they function as sample-

to-answer method through visual observation of the color change in the test zone. Several quantitative LFIA techniques have been broadly developed, however, these assays rely on optical or electrochemical techniques which still requires external instruments like optical analyzer, potentiostats, or even smartphone for signal readout. This increases the cost of analysis and may be challenging to operate for an unskilled user. Furthermore, the approach utilizes biorecognition substrate like antibodies and enzymes, which may compromise assay stability under environmental conditions due to their poor stability and this may result in false-negative outcomes.[12-14] Therefore, the development of an instrument-free and portable analytical sensor for quantitative measurement of cytokine levels is highly desirable for point-of-care (POC) testing.

Distance-based paper analytical devices (dPADs) have garnered significant attention as a promising analytical tool for POC applications.[15-17] The signal readout is straightforward through a naked-eye measurement of a distance length of a color change along a reaction channel where the analyte can react with a deposited reagent. The device consumes minimal sample and reagent volumes in the microlite level.[18,19] Moreover, sample fluid is transported naturally through the capillary forces on paper without the need for an external pump. The extent of the distance length provides a quantitative detection proportional to the analyte concentration.[20-22] With these characteristics, this measurement format is simpler than colorimetric, fluorescent, and electrochemical techniques, and also can be operated by untrained individuals. Furthermore, this technique can reduce errors that are common in colorimetric and fluorescent measurements from ambient lighting or background autofluorescence.[23,24] Previously, members of our group successfully developed a dPAD immunosensor for quantifying interleukin-6 (IL-6) in human samples utilizing methylene blue (MB) coated on the detection channel on paper.[7] The approach

88 integrates microfluidic principles, microfabrication techniques, and immunological strategies to
89 reduce the complexity and the time of the analysis procedure compared to traditional
90 immunoassay method. Although the assay achieved high sensitivity with a LOD of 50.0 fg mL^{-1}
91 by using naked-eye readout, it needed two antibodies for the assay development, leading to
92 increased analysis costs and storage concerns due to lower stability of the antibodies serving as
93 biorecognition substrates. Thus, there is still a need for a better sensitive and selective dPAD,
94 that does not rely on immunoassay approach and provides rapid and cost-effective measurements
95 of cytokine levels in biological fluids.

96 Molecularly imprinted polymers (MIPs) have received considerable attention as
97 promising alternatives to biorecognition elements such as antibodies, offering distinct advantages
98 of enhanced chemical and physical stability, and more straightforward production process.[25-28]
99 The principle behind MIP technology involves the use of molecular templates to generate
100 selective binding sites within cross-linked polymers, leading to the creation of specific
101 recognition binding sites for target analytes.[29-32] Interestingly, Tomas et al.[33] successfully
102 developed the dPADs integrated with MIP technique for chymotrypsinogen determination in
103 human urine samples. Their approach used dopamine as a monomer for surface imprinting onto
104 the detection channel due to its simple self-polymerization to form a polydopamine. The
105 quantitative analysis was based on the reaction between fluorescamine dry and the amino group
106 of the target protein absorbed into the MIP layer in the detection channel. While their assay can
107 selectively determine target protein concentration through distance measurement, the detection
108 procedure requires spraying of the fluorescamine solution on the entire detection area. It is
109 important to note that this fluorescent dye is dissolved in an organic solvent which can be
110 harmful for human health upon inhalation. More, this approach may result in error during signal

measurement caused by the reaction between the fluorescamine and the amino groups of polydopamine.[34] To address these limitations, the development of biocompatible and simpler dPAD combined using MIP for simpler detection with better signal-to-noise measurement is highly needed.

Herein, we introduce an innovative concept integrating dPAD with MIP technology and fluorescent carbon nanomaterials for cytokine biomarker quantification in human samples. Our aim is to design and fabricate the microfluidic device for simultaneous monitoring C-reactive protein (CRP), Tumor Necrosis Factor-alpha (TNF-α), and IL-6 which are all well-known biomarkers for the diagnosis and prognosis of cytokine-related diseases and chronic conditions.[35-37] In this work, the dPAD sensor was constructed of three connected zones, consisting of pretreatment, detection, and waste zones, for each of the biomarkers all sharing the sample zone. In the detection area, we pre-immobilized carbon dots (CDs) serving as fluorescent nanomaterial, chosen for their excellent optical stability and biocompatibility.[30,38] MIP layer of polydopamine for each biomarker was created by surface imprinting technique. Upon sample introduction to the sample zone of the device, the fluid immediately flows into the detection zone, where the fluorescence of the CDs is quenched along the distance length caused by the photo-induced electron transfer (PET) principle. With this distance readout, our developed dPADs can effectively monitor trace cytokine biomarkers in human samples with exceptional accuracy and precision. Overall, this strategy employing MIP and CDs with distance readout shows a significant promise for sensing of a broader spectrum of biomarkers for point of care diagnostics.

Experimental Section

Materials and Instruments

134 C-reactive protein (CRP) and human tumor necrosis factor-α human (TNF-α) were
135 bought from Sigma-Aldrich (USA). Human interleukin-6 (IL-6) was purchased from Abcam
136 company (UK). Dopamine hydrochloride, critic acid, ethylenediamine, carboxymethylcellulose
137 sodium (CMC), N-hydroxysulfosuccinimide sodium (NHS), (1-ethyl-3-(3-dimethylaminopropyl)
138 carbodiimide hydrochloride) (EDC), and acetic acid were obtained from Sigma-Aldrich (USA).
139 Bovine serum albumin (BSA), creatinine, cortisol, fructose, glucose, lactic acid, uric acid, and
140 bromophenol blue (BPB) were purchased from Sigma-Aldrich (USA). Urea was bought from
141 Fisher Scientific Company (USA). Tris(hydroxyamino)methane (tris), 2-(N-Morpholino)
142 ethanesulfonic acid hemisodium salt (MES), sodium hydroxide (NaOH), hydrochloric acid
143 (HCl), dibasic sodium phosphate (Na_2HPO_4), monobasic sodium phosphate (NaH_2PO_4),
144 potassium dihydrogen phosphate (KH_2PO_4), potassium bicarbonate ($KHCO_3$), sodium chloride
145 (NaCl), magnesium chloride ($MgCl_2$), calcium chloride ($CaCl_2$), sodium carbonate (Na_2CO_3),
146 and ascorbic acid were acquired from Sigma-Aldrich (USA). Preparation of phosphate buffer
147 solution (PBS), tris-HCl buffer solution (25.0 mmol L^{-1}, pH 8.5), artificial saliva, and sweat were
148 described in "Supplementary File".[7,39] All chemicals used in the experiment were of analytical
149 reagent (AR grade) and the solutions were prepared using PBS (50.0 mmol L^{-1}, pH 7.5). Human
150 control serum (heat inactivated from human male AB plasma, USA origin, sterile-filtered),
151 human serum (CRP) (ERM, certified reference material), and human control urine (Surine™
152 negative urine control samples) were acquired from Sigma-Aldrich (USA). Whatman No.1 filter
153 paper was obtained from GrowingLabs (USA). A household microwave oven (EM720CPN-
154 PMB, China) was employed for CDs synthesis. UV-visible spectrometer (Lambda 35, Perkin15
155 Elmer Instruments, USA), fluorescence spectroscopy (F-2500 Hitachi), Scanning Electron
156 Microscope (SEM, Axia ChemiSEM), Fourier-transform infrared spectroscopy (FT-IR, Nicolet

157 6700), and Transmission Electron Microscope (TEM, Titan Themis 300, 300 kV) were
158 performed for the assay characterizations. Design and fabrication of the UV-light black chamber
159 are shown and described in **Fig. S1** in "Supplementary File".

160 *Synthesis of CDs*

161 The CDs employed in the work were synthesized in accordance with a simple one-step
162 microwave technique.[38] Concisely, 2.0 g of citric acid was introduced to 5.0 mL of ultrapure
163 water and the solution was centrifuged for 10 min. Thereafter, 390.0 μL of ethylenediamine was
164 added into the as-prepared solution. Next, the mixture solution was put in the microwave at 700
165 W for 3 min. Then, the obtained red brown solid was purified by using a centrifugal filter unit
166 (Nanosep with 3.0 kDa) and diluted with ultrapure water. The CDs solution was stored at 4 C
167 before use. The characterization of the synthesized CDs was performed using fluorescence
168 spectrophotometer and TEM image indicated and discussed in **Fig. S2**.

169 *Preparation of MIPs Solution*

170 In brief, the dopamine solution was prepared by dissolving a tris-HCl buffer (25.0 mmol
171 L^{-1}, pH 8.5). Each template molecules of CRP (40.0 μg mL^{-1}), TNF-α (10.0 μg mL^{-1}), and IL-6
172 (30.0 μg mL^{-1}) were mixed with each dopamine solution in a 1:1 (v/v) ratio. Finally, the prepared
173 MIP solutions were used immediately. Non-imprinted polymer (NIP) was carried out using the
174 same procedure but without the template molecules.

175 *Device Fabrication and Operation*

176 First, the paper pattern was designed using Adobe Illustrator software program with a
177 sample zone (diameter 10.0 mm), three buffer pretreatment zones (diameter 5.0 mm), three
178 straight detection zones of 2.0 x 40.0 mm (width x length) with a 1.0 mm thick line inside, 1.0

179 mm apart, and three waste zones (diameter 6.0 mm). The total size of the paper sheet was 34.0
180 mm x 68.0 mm (width x length). After that, the designed paper was printed on Whatman No.1
181 filter paper using a wax printer (Xerox ColorQube, Japan). Subsequently, the printed paper was
182 beaked at 120 °C for 2.0 min and then cooled at room temperature. Next, the back side of them
183 was sealed with adhesive tape to avoid the solution leaking through the device. Afterwards, a
184 single drop at 3.0 μL of PBS (50.0 mmol L^{-1}, pH 7.5) and 6.0 μL of CMC (2.0 mg mL^{-1}) were
185 deposited onto the pretreatment zones and the detection zones, respectively, by dragging method
186 (**Scheme 1(a)**). Then, a single drop at 6.0 μL of CDs solution (2.0 mg mL^{-1}) were coated onto
187 the detection zone and attained to dry at room temperature (**Scheme 1(b)**). Subsequently, a single
188 drop at 6.0 μL of each prepared MIP solution for CRP, TNF-α, and IL-6 was immobilized onto
189 each detection zone and let to stand at room temperature for 15 min to form a MIP layer on the
190 paper surface (**Scheme 1(c)**). Later, the template removal was conducted by pipetting 3 x 6.0 μL
191 of 1.0% acetic acid to break down the hydrogen bond interaction between dopamine and
192 template molecules, and then 3 x 6.0 μL of DI water was pipetted to remove the rest of the acetic
193 acid (**Scheme 1(d)**). Finally, a single drop at 6.0 μL of the mixture solution of EDC (5.0 mg mL^{-}
194 ^{1}) and NHS (5.0 mg mL^{-1}) was introduced onto the detection zone to block amino groups of
195 polydopamine and then let it stand at room temperature until it has thorough dried. The CMC
196 and CDs concentrations were optimized and described in **Fig. S3** and **Fig. S4**.[40] Moreover, the
197 characteristics of the proposed dPADs were investigated using SEM image as shown and
198 described in **Fig. S5-S7**.[28,30,38,41-43]

199 *General Optimization and Analytical Procedure*

200 To fully optimize the developed dPADs, 60.0 μL of solution containing CRP (2.50 pg
201 mL^{-1}), TNF-α (0.25 pg mL^{-1}), and IL-6 (1.50 pg mL^{-1}) was used in all conditions by introducing

202 it into the sample zone of the device. Subsequently, we let it stand at room temperature for 40
203 min to allow for the diffusion of analytes to the detection zone with a capillary action. Lastly, the
204 distance length of the apparent fluorescence quenching was measured under UV light in a black
205 chamber by a traditional ruler with the resolution of being at 0.50 mm. All experiments were
206 performed in triplicate (n = 3).

207 The analytical efficiency was studied by adding 60.0 μL of solution containing a different
208 concentration of CRP, TNF-α, and IL-6 into the sample zone. Similarly, the procedure was
209 carried out according to the above-mentioned. The LODs were determined by measuring their
210 lowest concentrations that can promote the distance signal change from the blank using naked-
211 eye observation. Reproducibility was studied by detecting these biomarkers at four different
212 levels and then calculated by the relative standard deviation at ten times (n = 10). Selectivity was
213 evaluated through the measurement of the distance signal of CRP (12.0 pg mL^{-1}), TNF-α (2.0 pg
214 mL^{-1}), and IL-6 (10.0 pg mL^{-1}) compared to the signal obtained from other substrates. The
215 interferent effects were further studied by mixing target biomarkers with interfering molecules
216 during measurement (n = 3).

217 *Real Sample Analysis*

218 The practicability of our developed dPADs was tested by the spiking method. Human
219 control serum, urine, artificial saliva, and sweat consisting of CRP, TNF-α, and IL-6 at their
220 different concentrations were introduced into the sample zone of the device and following all the
221 steps for readout and measurement. The percentage of recovery was subsequently calculated
222 through the measurement of these target analyte concentrations in all control samples.

223 **Results and Discussion**

224 *Working Principle and Feasibility Tests*

225 The dPAD sensor for simultaneous CRP, TNF-α, and IL-6 detection utilizing CDs and
226 MIP relies on the electronic transfer caused by fluorescence quenching after surface absorption
227 of target analyte.[23,24] CDs generally absorb UV energy through their free electrons, allowing
228 them to become excited. As these excited electrons revert to their ground state, they emit blue
229 fluorescence. When the target analytes selectively bind to MIP layer through hydrogen bonding
230 interaction and Van der Waals forces,[29,33] it leads to PET between the target analytes and the
231 CDs, resulting in the quenching of their fluorescence emission.[27,28,30,41] Similarly, the quenching
232 system in this technique is categorized as dynamic quenching.[44,45] To verify this interaction on
233 the developed device, we tested whether the fluorescence emission of the CDs can be changed
234 when analytes were bound to their MIP layers and also removed. Upon exposure to UV light, the
235 detection zone initially exhibits bright fluorescence (**Fig. 1(a)**). When a sample solution
236 containing CRP, TNF-α, and IL-6 is added into the sample zone, it immediately flowed to the
237 detection zone via the capillary action. At this point, the analytes selectively bind to the MIP
238 cavities in their detection channels, while other molecules are transported to the waste zone. The
239 fluorescence quenching rapidly appeared along the detection zone where the concentration of
240 target analytes can be qualified by measuring this distance length. After removing the templates,
241 the fluorescence of the CDs returned to its initial brightness. Thus, we could confirm that our
242 developed dPADs allowed for the selective monitoring of target analytes.

243 We further tested the feasibility of our device through the detection of the distance
244 signals in the presence of MIP and NIP for simultaneous detection of CRP (12.0 pg mL^{-1}), TNF-
245 α (2.0 pg mL^{-1}), and IL-6 (10.0 pg mL^{-1}). **Fig. 1(b)** illustrates the resulting distance signals
246 obtained from different imprints coated onto each detection zone of the device. With all MIP

247 templates present for these analytes, the distance signals of 0.0 mm were obtained when exposed
248 to the blank solution (**Fig. 1(b; A)**). Conversely, they were 12.67, 24.67, and 21.33 mm for CRP,
249 TNF-α, and IL-6, respectively (**Fig. 1(b; B)**). When MIP for CRP and NIPs for TNF-α and IL-6
250 were coated on their specific channels, only distance signal of 12.33 mm was observed in the
251 CRP detection zone, while TNF-α and IL-6 detection zones displayed 0.0 mm distance signals
252 (**Fig. 1(b; C)**). It can be noted that the distance value for both assays was still consistent. Similar
253 behavior was acquired for TNF-α and IL-6 when their MIPs were only applied to their specific
254 channels (**Fig. 1(b; D and E)**), confirming that there was no significant interference between the
255 analytes. More interestingly, when NIPs were immobilized in all detection zones, the distance
256 signals were 0.0 mm (**Fig. 1(b; F)**). Since our method quantifies fluorescence change through
257 distance (and not intensity) measurements, there is no background interference as in a
258 conventional fluorescent intensity measurement-based system. Additionally, the target analytes
259 possibly flow to the waste zone via capillary action which did not absorb on MIP layer in the
260 detection zone. Lack of background signal and simplicity of measurement imparts our device
261 with more benefits over previous MIP techniques that rely on fluorescent intensity measurement
262 using specialized readers.

263 *Effect of Sample Volume and Reaction time*

264 The influence of the sample volumes is significant to microfluidic analysis since they are
265 associated with the amount of the target mole analyte presents in the solution.[20-23] We studied
266 sample volumes between 30.0 and 90.0 μL containing CRP (12.0 pg mL^{-1}), TNF-α (2.0 pg mL^{-}
267 ^{1}), and IL-6 (10.0 pg mL^{-1}), then monitored the quenched fluorescence distance signals as shown
268 in **Fig. 2(a)**. The distance signals gradually increased between 30.0 and 50.0 μL for CRP and
269 TNF-α but reached 60.0 μL for IL-6 measurement. Afterward, the distance signals remained

270 constant until the sample volume reached 70.0 μL. Beyond this point, there was a significant
271 decline in distance signals due to the potential for an overloaded sample volume to lead to
272 leakage from the sample zone and then unable to flow through the microchannel. We therefore
273 selected the sample volume of 60.0 μL as an appropriate level for our method. The effect of
274 dopamine and template concentration, polymerization time, pH, and storage time of the proposed
275 dPADs were studied and described in **Fig. S8-S11** in "Supplementary file".[25,26,31] Likewise, we
276 analyzed the reaction time between 20 and 60 min using a timer after introducing the solution in
277 the sample zone. **Fig. 2(b)** indicated that the distance signals rose with the reaction time up to 40
278 min for CRP and IL-6 and 35 min for TNF-α, and then plateaued. We also observed that the
279 fluidic solution fully traveled to waste zone for at least 40 min (**Fig. S12**). This result is
280 consistent to the previous method to simultaneous quantification of biomolecules and metal ions
281 using dPAD.[15,22,24] So, the reaction time of 40 min was chosen in our method for the multiplexed
282 monitoring of these analytes. Besides, our device could be reused at least five times as shown in
283 the result in **Fig. S13**. Consequently, our sensor shows the potential as a reusable, stable, and
284 cost-efficient analytical method for rapid POC monitoring, that can be performed by unskilled
285 users in resource limited settings.

286 *Analytical Characteristics*

287 The analytical performance of the proposed dPAD sensor for the quantitative detection of
288 CRP, TNF-α, and IL-6 was investigated under optimal conditions. The assays were performed
289 with both the blank solution and the solutions containing varying biomarker concentrations.
290 When the blank solution was introduced, the whole detection zone remained brightly fluorescent
291 (**Fig. 3(a)**). While some of the fluorescence distance length on the detection zone turned off
292 when the solution containing CRP (2.50 pg mL^{-1}), TNF-α (0.25 pg mL^{-1}), and IL-6 (1.50 pg mL^{-}

293 [1]) was introduced into the sample zone of the sensor (**Fig. 3(b)**). Furthermore, we observed exact
294 increments in the distance signals within the detection zone, directly proportional to the
295 concentrations of these analytes, as shown in **Fig. 3(b)~(j)**. The linear range for the
296 quantification was established in the range of 2.50-24.0 pg mL^{-1} (R^2 = 0.9974) for CRP, 0.25-
297 3.20 pg mL^{-1} (R^2 = 0.9985) for TNF-α, and 1.50-16.0 pg mL^{-1} (R^2 = 0.9966) for IL-6, as
298 indicated in **Fig. 3(k)**. We determined the limit of detections (LODs) for monitoring these
299 analytes by visually identifying the shortest distance signals that triggered quenched fluorescence
300 within the detection zone of the dPADs. We found that the distance signals were 1.0 mm when
301 the solution containing CRP (2.50 pg mL^{-1}), TNF-α (0.25 pg mL^{-1}), and IL-6 (1.50 pg mL^{-1})
302 were introduced. This measurement was repeated ten times (n = 10) to calculate signal
303 uncertainty and confirm our LODs.[46,47] The average distance signals of CRP at 2.50 pg mL^{-1},
304 TNF-α at 0.25 pg mL^{-1}, and IL-6 at 1.50 pg mL^{-1} were 1.0 mm, 0.9 mm, and 1.2 mm
305 respectively, while the average distance signal of the blank signal was 0.0 mm. The uncertainty
306 measurement of these levels was calculated as being at a 99% confident interval, which was 1.0
307 ± 0.48 mm for CRP, 0.90 ± 0.33 mm for TNF-α, and 1.2 ± 0.43 mm for IL-6, allowing a clear
308 distinction from the blank signal. We can hence ensure that the LODs for this developed dPAD
309 sensor are 2.50 pg mL^{-1} for CRP, 0.25 pg mL^{-1} for TNF-α, and 1.50 pg mL^{-1} for IL-6. These
310 LODs fall below the clinically relevant ranges for CRP (<200.0 μg mL^{-1}),[36] TNF-α (28.0-38.0 pg
311 mL^{-1}),[6] and IL-6 (5.0-15.0 pg mL^{-1})[7] detection in human biological samples, confirming that our
312 sensor can sensitively monitor these cytokine biomarkers. Specially, this technique demonstrated
313 the substantial binding affinity with the equilibrium dissociation constant (K_d) of 13.35, 1.67,
314 and 8.55 pg mL^{-1} for CRP, TNF-α, and IL-6, respectively, as calculations are described in
315 "Supplementary File".[31] Additionally, our method exhibits high precision with a maximum

316 relative standard deviation (RSD) of 5.14% (**Fig. S14**). We also found that our sensor was highly
317 selective and there was no interference as described in **Fig. S15**. Furthermore, our developed
318 dPADs offer a highly practical approach to monitoring compared to previous methods, as
319 indicated in **Table 1**. [6,7,10,11, 35-37,48-55] Though some of these prior methods employ techniques
320 such as resonance Raman, immunosensing, and photothermal detection that can exhibit greater
321 sensitivity than our method, it is important to note that they still need expensive instrumentation
322 and rely on expensive antibodies for biorecognition. On the other hand, our dPADs present an
323 instrument-free analytical sensor for timely monitoring of associated cytokine levels for clinical
324 POC testing. To the best of our knowledge, this is the first time a dPAD has been fabricated for
325 multiplexed sensing of CRP, TNF-α, and IL-6 without an immunological approach.

326 *Application in Real Samples*

327 We validated the practical performance of the developed dPADs for biomedical and
328 diagnostic applications using various human sample matrices, including control urine, control
329 serum, artificial saliva, and artificial sweat. Initially, we observed that distance signals for all
330 sample matrices without target analytes were 0.0 mm, similar to the blank signal. Subsequently,
331 we spiked standard levels of CRP, TNF-α, and IL-6 into these samples, and introduced them into
332 the dPADs. In **Table 2, Table 3**, and **Table 4**, the resultant recoveries ranged from 99.22% to
333 103.58%, with the highest RSD at 7.87%. Additionally, it can be noticed that the different
334 sample matrices did not affect our proposed sensor. As indicated in **Fig. S16**, the distance signals
335 of these biomarkers in four-different sample matrices were dramatically consistent. We also
336 tested effect of 10-fold dilute and undiluted serum solution by comparing the distance signals
337 obtained between those solutions. **Fig. S17** revealed the distance signals obtained from both
338 diluted and undiluted serum solution were significantly similar, showing that our sensor enables

339 to the serum samples without any dilution. More, we used our sensor to quantify the CRP level
340 in certified reference human serum in order to confirm the assay accuracy. The human serum
341 was diluted to fit within our linear range and then it was introduced into the dPAD sensor. **In**
342 **Table S1,** we found that the result obtained from our method was consistent to the reference
343 materials by a statical t-test calculation ($T_{critical}$ = 4.30). Consequently, the developed dPAD
344 sensor exhibits accurate and precise quantification of cytokine biomarkers in various sample
345 matrices, and it can be extended to other biomarkers to diagnose diseases across a broad
346 spectrum.

347 **Conclusion**

348 In this article, we present inexpensive dPADs for simultaneous quantification of cytokine
349 biomarkers, including CRP, TNF-α, IL-6 in human samples. By integrating MIP and CDs, the
350 quantitative measurement involves simply measuring the distance length of the quenched
351 fluorescence within the detection zone. The total analysis time of this assay was just 40 min for
352 simultaneous detection of three biomarkers, which is quite competitive compared to the state-of-
353 the-art methods. Interestingly, our sensor shows great selectivity compared to non-response in
354 the case of non-imprinted polymer, rendering a distinct advantage of cost and scalability over
355 previous methods relying on antibodies or aptamers. Furthermore, the sensor can be used to
356 monitor cytokine biomarkers within the clinically relevant range in various sample matrices. On
357 the whole, with the analytical performance, our developed sensing holds a great promise for
358 rapid diagnosis and prognosis for POC monitoring in resource-limited settings. Moreover, the
359 technique can be applied for quantification of other biomarkers for which the MIP layer can be
360 potentially adapted, demonstrating further opportunities for the analytical approach.

361 **Associated content.**

362 Supporting Information Available: Details of the solution preparation, 3D-printed UV-
363 light black chamber fabrication, surface characterization, CDs characteristics and optimization,
364 effect of CMC, dopamine, and template concentration, effect of polymerization time, pH, storage
365 time, reproducibility studies, selectivity and interferent studies, image of BSA-BPB complex in
366 waste zone, effect of sample matrices, binding constant calculation, and the result for CRP
367 detection in certificate reference human serum material.

368 **Conflicts of interest**

369 There are no conflicts to declare.

370 **Author contributions**

371 **Kawin Khachornsakkul**: Conceptualization, Methodology, Investigation, Validation,
372 Data curation, Project administration, Visualization, Writing - original draft, review, and editing.
373 **Ruben Del-Rio-Ruiz**: 3D UV-lamp box fabrication, Writing - review & editing. **Lita Chheang**:
374 SEM characterization. **Wenxin Zeng**: SEM characterization **Sameer Sonkusale**: Resources,
375 Project administration, Writing - review & editing.

376 **References**

377 1 F. C. Jammes and S. J. Maerkl, *Microsystems Nanoeng. 2020 61*, 2020, **6**, 1–14.
378 2 P. Jiang, Y. Zhang, B. Ru, Y. Yang, T. Vu, R. Paul, A. Mirza, G. Altan-Bonnet, L. Liu,
379 E. Ruppin, L. Wakefield and K. W. Wucherpfennig, *Nat. Methods 2021 1810*, 2021, **18**, 1181–
380 1191.
381 3 C. Liu, D. Chu, K. Kalantar-Zadeh, J. George, H. A. Young and G. Liu, *Adv. Sci.*, 2021,
382 **8**, 2004433.

383 4 F. A. Bozza, J. I. Salluh, A. M. Japiassu, M. Soares, E. F. Assis, R. N. Gomes, M. T.
384 Bozza, H. C. Castro-Faria-Neto and P. T. Bozza, *Crit. Care*, 2007, **11**, 1–8.
385 5 A. J. A. Lambeck, A. P. G. Crijns, N. Leffers, W. J. Sluiter, K. A. Ten Hoor, M. Braid, A.
386 G. J. Van Der Zee, T. Daemen, H. W. Nijman and W. M. Kast, *Clin. Cancer Res.*, 2007, **13**,
387 2385–2391.
388 6 A. S. Akhtar, R. R. G. Soares, I. F. Pinto and A. Russom, *Anal. Chim. Acta*, 2023, **1245**,
389 340823.
390 7 K. Khachornsakkul, W. Dungchai and N. Pamme, *ACS Sensors*, 2022, **7**, 2410–2419.
391 8 D. M. Del Valle, S. Kim-Schulze, H. H. Huang, N. D. Beckmann, S. Nirenberg, B.
392 Wang, Y. Lavin, T. H. Swartz, D. Madduri, A. Stock, T. U. Marron, H. Xie, M. Patel, K.
393 Tuballes, O. Van Oekelen, A. Rahman, P. Kovatch, J. A. Aberg, E. Schadt, S. Jagannath, M.
394 Mazumdar, A. W. Charney, A. Firpo-Betancourt, D. R. Mendu, J. Jhang, D. Reich, K. Sigel, C.
395 Cordon-Cardo, M. Feldmann, S. Parekh, M. Merad and S. Gnjatic, *Nat. Med. 2020 2610*, 2020,
396 **26**, 1636–1643.
397 9 G. Liu, M. Qi, M. R. Hutchinson, G. Yang and E. M. Goldys, *Biosens. Bioelectron.*,
398 2016, **79**, 810–821.
399 10 D. Y. Kong, N. S. Heo, J. W. Kang, J. B. Lee, H. J. Kim and M. Il Kim, *Anal. Bioanal.*
400 *Chem.*, 2022, **414**, 3257–3265.
401 11 D. Huang, H. Ying, D. Jiang, F. Liu, Y. Tian, C. Du, L. Zhang and X. Pu, *Anal.*
402 *Biochem.*, 2020, **588**, 113468.
403 12 R. Tang, H. Yang, J. R. Choi, Y. Gong, J. Hu, S. Feng, B. Pingguan-Murphy, Q. Mei and
404 F. Xu, *Talanta*, 2016, **152**, 269–276.
405 13 C. Srisomwat, A. Yakoh, N. Chuaypen, P. Tangkijvanich, T. Vilaivan and O.

Chailapakul, *Anal. Chem*., 2021, **93**, 2879–2887.

14 K. Kunpatee, M. Panphloi, K. Charoenkitamorn, U. Pimpitak, S. Puthong, A. Buakeaw, K. Komolpis, M. M. Sain, A. Yakoh and S. Chaiyo, *Sensors Actuators B Chem*., 2024, **401**, 135042.

15 R. Hiraoka, K. Kuwahara, Y. C. Wen, T. H. Yen, Y. Hiruta, C. M. Cheng and D. Citterio, *ACS Sensors*, 2020, **5**, 1110–1118.

16 K. Khachornsakkul, J. J. Chang, P. H. Lin, Y. H. Lin, W. Dungchai and C. H. Chen, *Anal. Chim. Acta*, 2021, **1154**, 338328.

17 X. Wei, T. Tian, S. Jia, Z. Zhu, Y. Ma, J. Sun, Z. Lin and C. J. Yang, *Anal. Chem.*, 2016, **88**, 2345–2352.

18 S. H. Al-Jaf and K. M. Omer, *Microchim. Acta*, 2022, **189**, 1–10.

19 S. H. Al-Jaf and K. M. Omer, *RSC Adv*., 2023, **13**, 15704–15713.

20 K. Khachornsakkul, A. Tiangtrong, A. Suwannasom, W. Sangkharoek, O. Jamjumrus and W. Dungchai, *Analyst*, 2022, **147**, 695–703.

21 D. M. Cate, W. Dungchai, J. C. Cunningham, J. Volckens and C. S. Henry, *Lab Chip*, 2013, **13**, 2397–2404.

22 D.M. Cate, S.D. Noblitt, J. Volckens, and C.S. Henry, *Lab Chip*, **2015**,15, 2808-2818.

23 M. Rahbar, B. Paull, and M. Macka,. *Anal. Chim. Acta* **2019**, 1063, 1–8.

24 K. Phoonsawat, K. Khachornsakkul, N. Ratnarathorn, C. S. Henry, and W. Dungchai, *ACS Sensors* **2021**, 6, 3047–3055.

25 Y. Ma, X. L. Shen, Q. Zeng, H. S. Wang and L. S. Wang, *Talanta*, 2017, **164**, 121–127.

26 S. Farooq, L. Xu, A. Ostovan, C. Qin, Y. Liu, Y. Pan, J. Ping and Y. Ying, *Food Chem.*, 2023, **429**, 136822.

429 27 J. Qi, B. Li, X. Wang, L. Fu, L. Luo and L. Chen, *Anal. Chem.*, 2018, **90**, 11827–11834.

430 28 B. Li, Z. Zhang, J. Qi, N. Zhou, S. Qin, J. Choo and L. Chen, *ACS Sensors*, 2017, **2**, 243–
431 250.

432 29 R. Keçili, C. G. Hussain and C. M. Hussain, *Trends Environ. Anal. Chem.*, 2023, **40**,
433 e00213.

434 30 S. Bhogal, I. Mohiuddin, S. Kumar, A. K. Malik, K. H. Kim and K. Kaur, *Sci. Total*
435 *Environ.*, 2022, **847**, 157356.

436 31 W. Jesadabundit, S. Jampasa, K. Patarakul, W. Siangproh and O. Chailapakul, *Biosens.*
437 *Bioelectron.*, 2021, **191**, 113387.

438 32 S. M. Pirot and K. M. Omer, *Microchem. J.*, 2022, **182**, 107921.

439 33 T. Rypar, V. Adam, M. Vaculovicova and M. Macka, *Sensors Actuators B Chem.*, 2021,
440 **341**, 129999.

441 34 K. Imai, *J. Chromatogr. A.* **1975***,* 105*,* 135-140.

442 35 C. Jiang, M. T. Alam, S. M. Silva, S. Taufik, S. Fan and J. J. Gooding, *ACS Sensors*,
443 2016, **1**, 1432–1438.

444 36 D. Hong, K. Kim, E. J. Jo and M. G. Kim, *Anal. Chem.*, 2021, **93**, 7925–7932.

445 37 J. Peng, J. Guan, H. Yao, and X. Jin, *Anal. Biochem.* **2016**, *492*, 63–68.

446 38 B. Ninwong, P. Sangkaew, P. Hapa, N. Ratnarathorn, R. F. Menger, C. S. Henry and W.
447 Dungchai, *RSC Adv.*, 2020, **10**, 9884–9893.

448 39 K. Midander, A. Julander, J. Kettelarij, and J. Liden, *Regul. Toxicol. Pharmacol.* **2016**,
449 81, 381-386.

450 40 K. Khachornsakkul and W. Dungchai, *Anal. Sci.*, 2020, 20P349.

451 41 M. Lim, S. P. Thanasupsin and N. Thongkon, *Molecules*, 2022, **27**, 7257.

42 Z. Zhang, X. Ma, M. Jia, B. Li, J. Rong, and X. Yang, *Analyst*, **2019**, 144, 1282–1291.

43 I.H. Mondal, S. Yeasmin, and S. Rahman, *Int. J. Biol. Macromol*. **2015**, *79*, 144-150.

44 F. Noun, E. A. Jury and R. Naccache, *Sensors*, 2021, **21**, 1391.

45 F. Zu, F. Yan, Z. Bai, J. Xu, Y. Wang, Y. Huang and X. Zhou, *Microchim. Acta*, 2017, **184**, 1899–1914.

46 K. Khachornsakkul and W. Dungchai, *ACS Sensors*, 2021, **6**, 1339–1347.

47 K. Khachornsakkul, R. Del-Rio-Ruiz, L. Chheang and S. Sonkusale, *Sensors Actuators B Chem.*, 2023, **395**, 134518.

48 R. Wu, S. Zhou, T. Chen, J. Li, H. Shen, Y. Chai and L. S. Li, *Anal. Chim. Acta*, 2018, **1008**, 1–7.

49 B. Wu, R. Jiang, Q. Wang, J. Huang, X. Yang, K. Wang, W. Li, N. Chen and Q. Li, *Chem. Commun.*, 2016, **52**, 3568–3571.

50 S. Jampasa, W. Siangproh, R. Laocharoensuk, T. Vilaivan and O. Chailapakul, *Talanta*, 2018, **183**, 311–319.

51 S. Laing, A. Hernandez-Santana, J. Sassmannshausen, D. L. Asquith, I. B. McInnes, K. Faulds and D. Graham, *Anal. Chem.*, 2011, **83**, 297–302.

52 H. Li, X. Li, L. Chen, B. Li, H. Dong, H. Liu, X. Yang, H. Ueda and J. Dong, *ACS Omega*, 2021, **6**, 31009–31016.

53 M. D. Gholami, P. Sonar, G. A. Ayoko and E. L. Izake, *Sensors Actuators B Chem.*, 2020, **310**, 127867.

54 R. Malhotra, V. Patel, J. P. Vaqué, and J. S. Gutkind, *Anal. Chem.* **2010**, 82, 3118–3123.

G. C. E. Keustermans, S. B. E. Hoeks, J. M. Meerding, B. J. Prakken, and W. de Jager, *Methods* **2013**, *61* (1), 10–17.

55 K. Khachornsakkul, R. Del-Rio-Ruiz, W. Zeng and S. Sonkusale, *Anal. Chem.*, **2023**, *95* (34), 12802–12810.

494 **Table 1**. Comparison of analytical performance between the developed technique and other

495 techniques for CRP, TNF-α, and IL-6 detection.

496

Analytes	Method	Linear range (pg mL^{-1})	LOD (pg mL^{-1})	Reference
CRP	Colorimetric	117.0 x 10^3 – 10.0 x 10^6	117.0 x 10^3	10
	Electrochemiluminescence	10.0 – 1000 x 10^3	4.60	36
	Fluorescent	500.0 – 1.0 x 10^6	300.0	48
	SRP-aptamer	10.0 – 100.0 x 10^3	10.0	49
	Electrochemical	10.0 x 10^3 – 150.0 x 10^6	1.50 x 10^3	50
	dPADs@CDs@MIPs	2.50 – 24.0	2.50	This work
TNF-α	Colorimetric	1.0 x 10^3 – 100.0 x 10^3	600.0	6
	Electrochemical	10.0-500 x 10^3	10.0	35
	Resonance Raman	0.049 – 0.195	0.09	51
	Fluorescent	250.0 – 250.0 x 10^3	123.0	52
	SERS	173.0 – 520.0 x 10^3	173.0	53
	dPADs@CDs@MIPs	0.25 – 3.20	0.25	This work
IL-6	dPADs immunosensor	0.05 – 25.0	0.05	7
	LFIA	2.0 – 5.0 x 10^2	370.0	11
	Magnetic colorimetric	0.10 – 1.0 x 10^4	40.0	37
	Electrochemical	0.50 – 5.0	500.0	54
	Photothermal	0.03 – 0.36	0.02	55
	dPADs@CDs@MIPs	1.50 – 16.0	1.50	This work

497

498

499

500

501

502

503

504 **Table 2**. Recovery studies of the detection of CRP in human biological samples (n = 3).

Sample type	CRP standard added. (pg mL^{-1})	Total found. ± S.D. (pg mL^{-1})	%Recovery	%RSD
Human serum	5.0	5.03 ± 0.29	100.67	7.87
	10.0	10.23 ± 0.58	102.28	5.59
	15.0	15.16 ± 0.58	101.09	3.46
	20.0	20.36 ± 0.58	101.79	2.47
Human urine	5.0	5.16 ± 0.29	103.26	7.53
	10.0	10.10 ± 0.76	100.98	7.51
	15.0	15.29 ± 0.29	101.96	1.71
	20.0	20.23 ± 0.29	101.14	1.25
Artificial saliva	5.0	5.03 ± 0.29	100.67	7.87
	10.0	10.36 ± 0.50	103.58	4.76
	15.0	15.42 ± 0.50	102.82	2.94
	20.0	20.62 ± 0.58	103.09	2.44
Artificial sweat	5.0	5.16 ± 0.29	103.23	7.53
	10.0	9.97 ± 0.50	99.69	5.00
	15.0	15.16 ± 0.58	101.09	3.76
	20.0	20.36 ± 0.58	101.79	2.47

505

506

507

508

509

510

511

512

513

514

515

516

517

518 **Table 3**. Recovery studies of the detection of TNF-α in human biological samples (n = 3).

Sample type	TNF-α standard added. (pg mL^{-1})	Total found. ± S.D. (pg mL^{-1})	%Recovery	%RSD
Human serum	1.0	1.03 ± 0.29	102.98	2.59
	1.5	1.49 ± 0.58	99.52	3.33
	2.0	2.02 ± 0.58	100.92	2.37
	2.5	2.49 ± 0.58	99.76	1.88
Human urine	1.0	1.00 ± 0.29	99.23	2.71
	1.5	1.52 ± 0.58	99.52	3.33
	2.0	2.04 ± 0.29	102.17	2.34
	2.5	2.54 ± 0.58	101.76	1.84
Artificial saliva	1.0	0.99 ± 0.29	99.23	2.71
	1.5	1.49 ± 0.58	99.52	3.33
	2.0	2.03 ± 0.50	101.55	2.04
	2.5	2.53 ± 0.29	101.26	0.93
Artificial sweat	1.0	1.02 ± 0.50	101.73	4.55
	1.5	1.53 ± 0.29	102.03	1.62
	2.0	2.03 ± 0.87	101.55	3.53
	2.5	2.54 ± 0.58	101.76	1.84

519

520

521

522

523

524

525

526

527

528

529

530

531

532 **Table 4**. Recovery studies of the detection of IL-6 in human control samples (n = 3).

Sample type	IL-6 standard added. (pg mL^{-1})	Total found. ± S.D. (pg mL^{-1})	%Recovery	%RSD
Human serum	6.0	5.95 ± 0.58	99.22	5.09
	9.0	9.32 ± 0.58	103.56	2.99
	12.0	11.99 ± 0.58	99.88	2.25
	15.0	15.21 ± 0.58	101.42	1.73
Human urine	6.0	6.29 ± 0.58	101.56	4.95
	9.0	9.25 ± 0.29	102.78	1.51
	12.0	12.06 ± 0.76	100.47	2.96
	15.0	15.00 ± 0.29	100.01	0.88
Artificial saliva	6.0	6.02 ± 0.50	100.39	4.35
	9.0	9.11 ± 0.58	101.22	3.07
	12.0	11.92 ± 0.50	99.30	1.96
	15.0	14.93 ± 0.58	99.55	1.77
Artificial sweat	6.0	5.95 ± 0.58	99.22	5.09
	9.0	9.11 ± 0.29	101.22	1.53
	12.0	11.99 ± 0.58	99.88	2.25
	15.0	15.00 ± 0.76	100.01	2.33

533

534

535

536

537

538

539

540

541

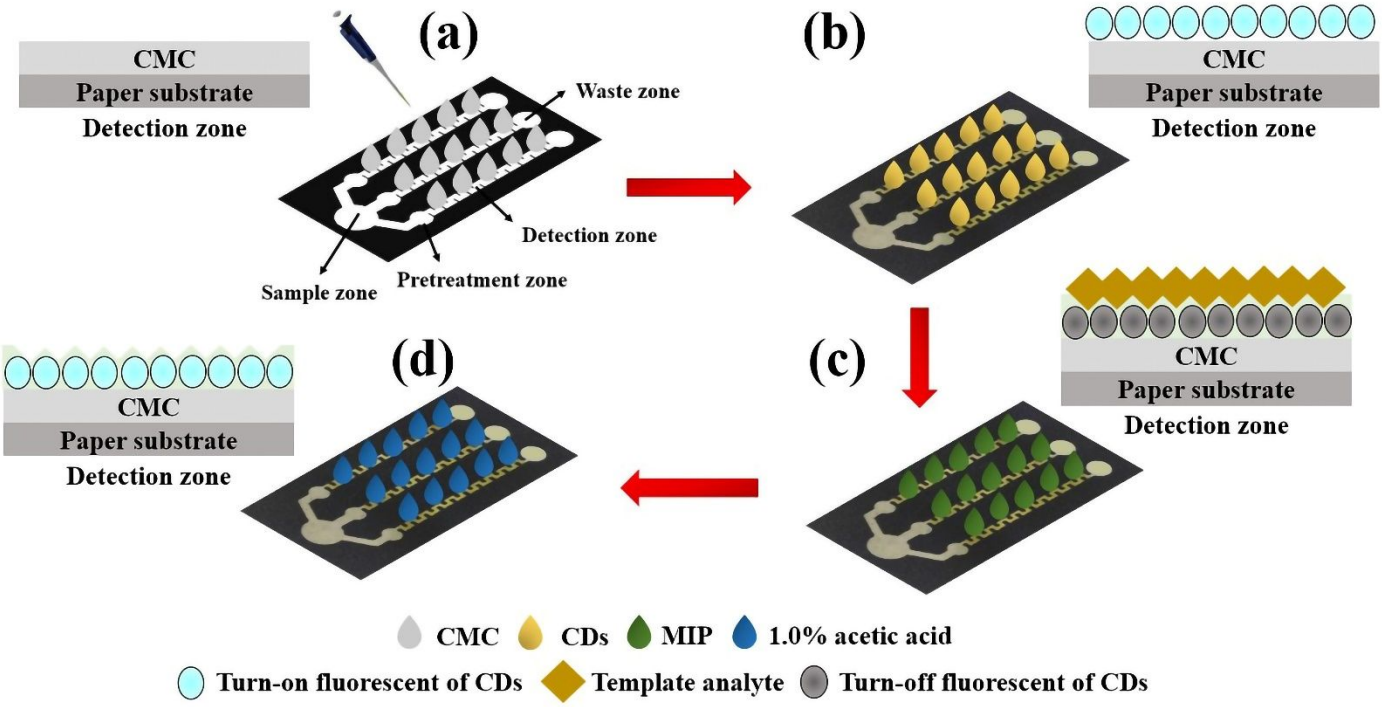

Scheme 1 Illustrate the dPAD fabrication using dragging technique of single drop of solution including, (a) CMC deposition, (b) CDs addition, (c) MIP immobilization, and (d) washing the template using acetic acid.

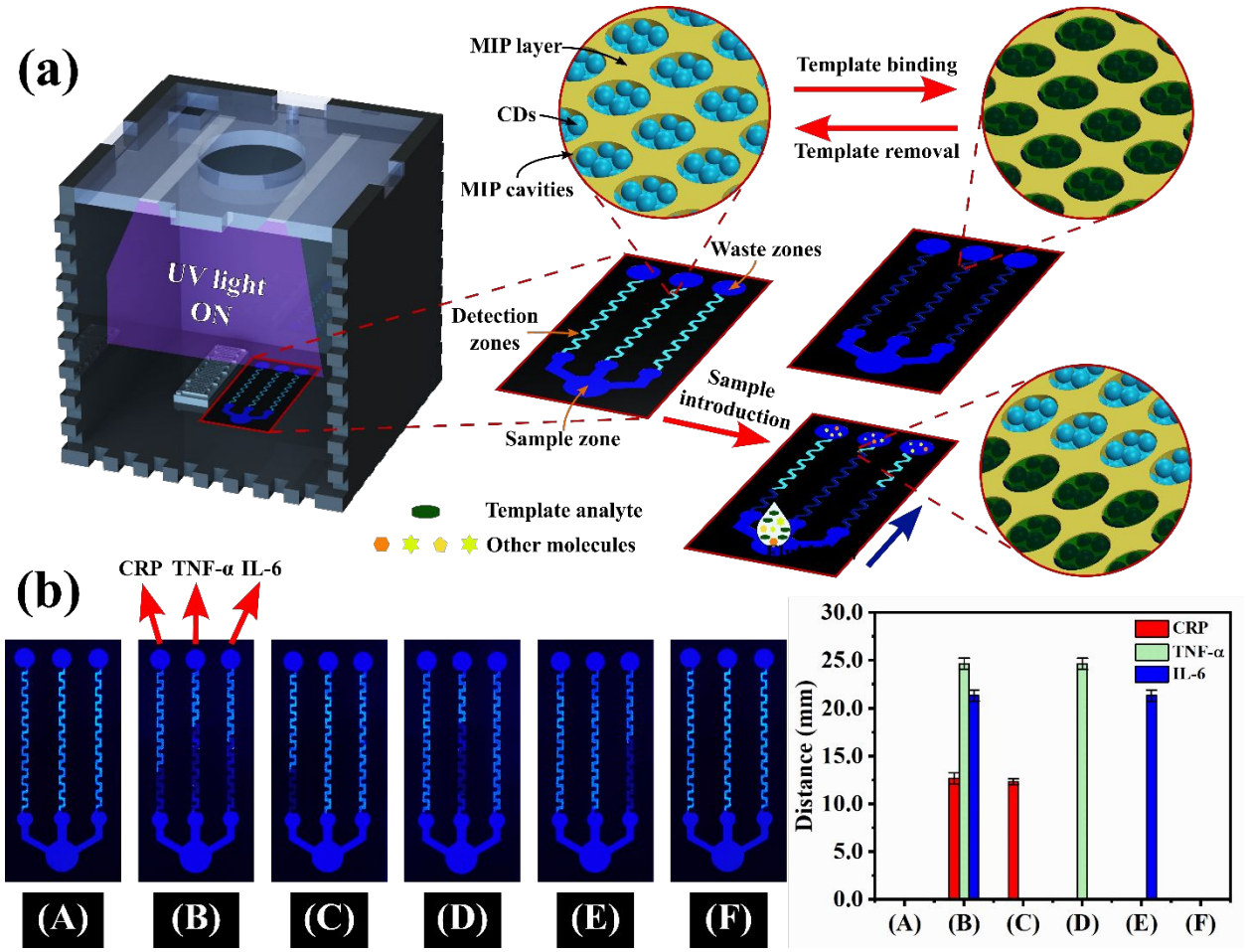

Fig. 1 Scheme of (a) the principle and workflow of the developed dPAD sensor, and (b) the distance signals of the presence of MIP templates of all analytes for the blank detection (A) and solution containing CRP (12.0 pg mL^{-1}), TNF-α (2.0 pg mL^{-1}), and IL-6 (10.0 pg mL^{-1}) (B), the presence of only MIP template for CRP (C), TNF-α (D), IL-6 (E), and the presence of NIP templates of all analytes (F) (n = 3).

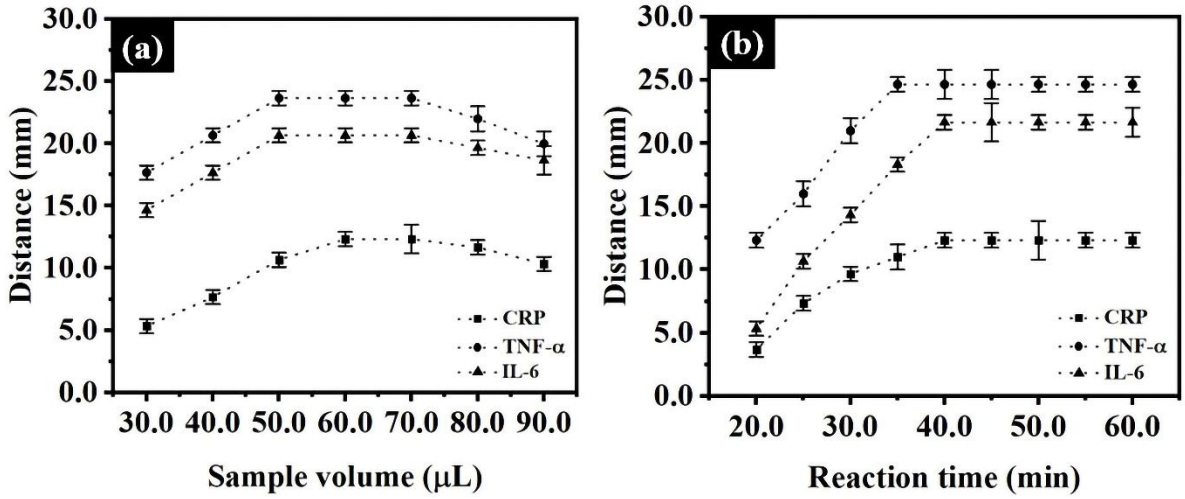

Fig. 2 Demonstrate the distance signals of (a) the sample volume and (b) reaction time for (■) CRP (12.0 pg mL^{-1}), (●) TNF-α (2.0 pg mL^{-1}), and (▲) IL-6 (10.0 pg mL^{-1}) detection in the developed dPADs (n = 3).

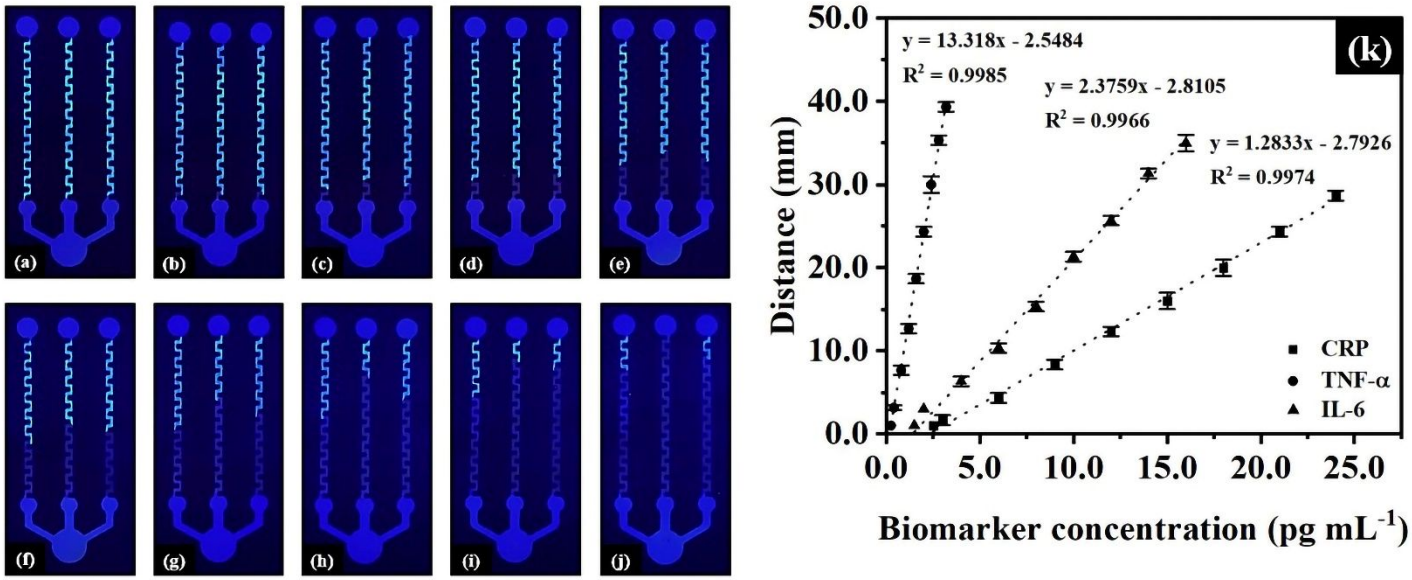

Fig. 3 Image of dPAD sensor for simultaneous measurement of CRP, TNF-α, and IL-6 containing (a) blank, (b) 2.50, 0.25, 1.50, (c) 3.0, 0.40, 2.0, (d) 6.0, 0.80, 4.0, (e) 9.0, 1.2, 6.0, (f) 12.0, 1.6, 8.0, (g) 15.0, 2.0, 10.0, (h) 18.0, 2.4, 12.0, (i) 21.0, 2.8, 14.0, and (j) 24.0, 3.2, 16.0 pg mL^{-1} for CRP, TNF-α, and IL-6, respectively. In (k) the linear line plotted with distance signals as a function for CRP, TNF-α, and IL-6 concentrations from 2.50 to 24.0, from 0.25 to 3.2, and from 1.50 to 16.0 pg mL^{-1} (n = 3).